



HAL
open science

Emergent constraint on Arctic Ocean acidification in the twenty-first century

Jens Terhaar, Lester Kwiatkowski, Laurent Bopp

► **To cite this version:**

Jens Terhaar, Lester Kwiatkowski, Laurent Bopp. Emergent constraint on Arctic Ocean acidification in the twenty-first century. *Nature*, 2020, 582 (7812), pp.379-383. 10.1038/s41586-020-2360-3. hal-02884111

HAL Id: hal-02884111

<https://hal.science/hal-02884111v1>

Submitted on 10 Nov 2020

HAL is a multi-disciplinary open access archive for the deposit and dissemination of scientific research documents, whether they are published or not. The documents may come from teaching and research institutions in France or abroad, or from public or private research centers.

L'archive ouverte pluridisciplinaire **HAL**, est destinée au dépôt et à la diffusion de documents scientifiques de niveau recherche, publiés ou non, émanant des établissements d'enseignement et de recherche français ou étrangers, des laboratoires publics ou privés.

1 Emergent constraint on Arctic Ocean
2 acidification in the twenty-first century

3 **Jens Terhaar^{1,2,3*}, Lester Kwiatkowski^{1,4}, Laurent Bopp¹**

4 ¹ LMD/IPSL, Ecole Normale Supérieure/PSL Université, CNRS, Ecole Polytechnique, Sorbonne
5 Université, Paris, France

6 ² Climate and Environmental Physics, Physics Institute, University of Bern, Switzerland

7 ³ Oeschger Center for Climate Change Research, University of Bern, Switzerland

8 ⁴ LOCEAN/IPSL, Sorbonne Université, CNRS, IRD, MNHN, Paris, France

9

10

11

12

13

14 ***Jens Terhaar**

15 **Climate and Environmental Physics, Physics Institute**

16 **University of Bern**

17 **Sidlerstrasse 5**

18 **3012 Bern**

19 **Switzerland**

20 **jens.terhaar@climate.unibe.ch**

21 The ongoing uptake of anthropogenic carbon by the ocean leads to ocean acidification, a
22 process that results in a reduction in pH and the saturation state of biogenic calcium
23 carbonate minerals ($\Omega_{\text{calc/arag}}$)^{1,2}. Due to naturally low $\Omega_{\text{calc/arag}}$ ^{2,3}, the Arctic Ocean is
24 considered the most susceptible region to future acidification and associated ecosystem
25 impacts^{4,5,6,7}. However, the magnitude of projected twenty-first century acidification differs
26 strongly across Earth System Models (ESMs)⁸. Here we identify an emergent multi-model
27 relationship between the simulated present-day density of Arctic Ocean surface waters, used
28 as a proxy for Arctic deep-water formation, and projections of the anthropogenic carbon
29 inventory and coincident acidification. Applying observations of sea surface density, we
30 constrain the end of twenty-first century Arctic Ocean anthropogenic carbon inventory to 9.0
31 ± 1.6 Pg C and basin-averaged Ω_{arag} and Ω_{calc} to 0.76 ± 0.06 and 1.19 ± 0.09 respectively,
32 under the RCP 8.5 climate scenario. Our results indicate greater regional anthropogenic
33 carbon storage and ocean acidification than previously projected^{3,8} and increase the
34 probability that large parts of the mesopelagic Arctic Ocean will be undersaturated with
35 respect to calcite by the end of the century. This increased rate of Arctic Ocean acidification
36 combined with rapidly changing physical and biogeochemical Arctic conditions^{9,10,11}, is likely
37 to exacerbate the impact of climate change on vulnerable Arctic marine ecosystems.

38

39

40

41 While the uptake of atmospheric carbon by the ocean mitigates climate change, it also
42 dramatically influences marine chemistry, decreasing pH and carbonate ion concentrations
43 $[\text{CO}_3^{2-}]$ and increasing concentrations of aqueous carbon dioxide and bicarbonate ions $[\text{HCO}_3^-]$
44 1,2 . These changes in seawater chemistry, collectively known as ocean acidification, have been
45 shown to negatively impact wide-ranging marine organisms including molluscs, crustaceans,
46 echinoderms, cnidarians and teleost fish^{4,5,6,7}. Calcifying marine organisms are particularly
47 sensitive to ocean acidification, which can impair their growth, reproduction and survival^{2,4,12}.
48 The thermodynamic stability of calcium carbonate is described by the calcium carbonate
49 saturation state ($\Omega = [\text{Ca}^{2+}][\text{CO}_3^{2-}]/K_{\text{sp}}$), with K_{sp} representing the relevant CaCO_3 solubility
50 product, and Ω_{calc} and Ω_{arag} representing the saturation state of the stable calcite and
51 metastable aragonite mineral forms, respectively. Ocean acidification acts to reduce Ω by
52 reducing carbonate ion concentrations. Studies have shown that as Ω decreases, calcification
53 rates at both the organism^{12,13,14} and community-level¹⁵ typically decline. In addition, the
54 corrosion of pure mineral forms is actively promoted under exposure to undersaturated
55 conditions ($\Omega < 1$).

56

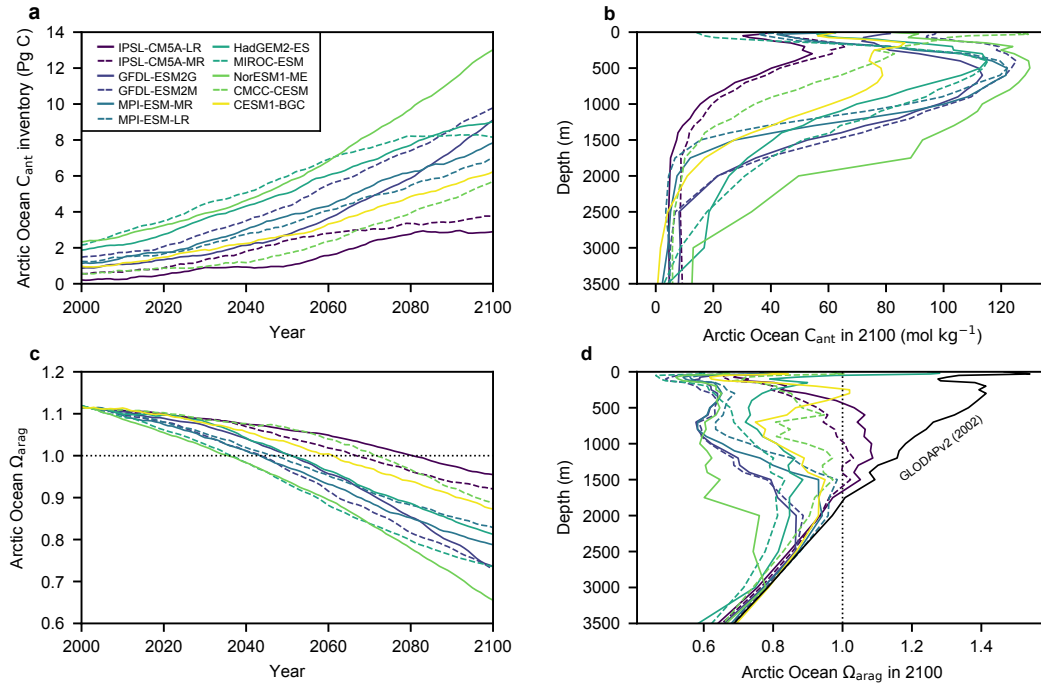
57 The Arctic represents the global region projected to experience the most severe climate
58 change, with polar amplification causing a projected end-of-century surface temperature
59 increase of up to 8.3 ± 1.9 °C¹⁰ and loss of summer sea-ice¹¹. The same is true for the Arctic
60 Ocean, where low temperatures and consequently the high solubility of CO_2 , result in naturally
61 low pH and $\Omega^{2,3}$. Given this natural state and the amplifying effect of climate change¹⁶, the

62 Arctic Ocean is projected to experience the lowest pH and Ω conditions in the coming decades³,
63 as well as dramatic changes in the temporal variability of marine chemistry⁹.

64

65 Projections by ESMs under the high-emissions Representative Concentration Pathway 8.5
66 (RCP8.5)¹⁷ suggest that the entire Arctic Ocean will be undersaturated with respect to aragonite
67 ($\Omega_{\text{arag}} < 1$) by the end of the twenty-first century (Fig. 1), while basin-wide calcite
68 undersaturation ($\Omega_{\text{calc}} < 1$) is not expected to occur this century^{3,8,18} (Extended Data Figure 1).
69 Projected changes in ocean chemistry are predominantly confined to the upper 2500 m of the
70 water column, with large model uncertainties persisting with regard to the end-of-century
71 anthropogenic carbon inventory (2.9-13.0 Pg C)¹⁹, and the associated average Ω_{arag} (0.66-0.95)
72 and Ω_{calc} (1.02-1.49)⁸. Although projection uncertainties are limited in the surface ocean²⁰, they
73 are highly pronounced at depth (Fig. 1 and Extended Data Figure 1) and complicate
74 assessments of likely impacts on vulnerable marine ecosystems⁷.

75



76

77 **Fig. 1. Projections of Arctic Ocean anthropogenic carbon and aragonite saturation state. a,** ESM
 78 projections of the twenty-first century Arctic Ocean anthropogenic carbon (C_{ant}) inventory and **c,** basin-
 79 averaged Ω_{arag} . Vertical profiles of **b,** basin-averaged anthropogenic carbon and **d,** Ω_{arag} in 2100 for the
 80 11 ESMs. The GLODAPv2²⁴ observational profile of Ω_{arag} for 2002 is marked as a black line in **d.** Arctic
 81 Ocean boundaries are the Fram Strait, the Barents Sea Opening, the Bering Strait and the Canadian
 82 Arctic Archipelago.

83

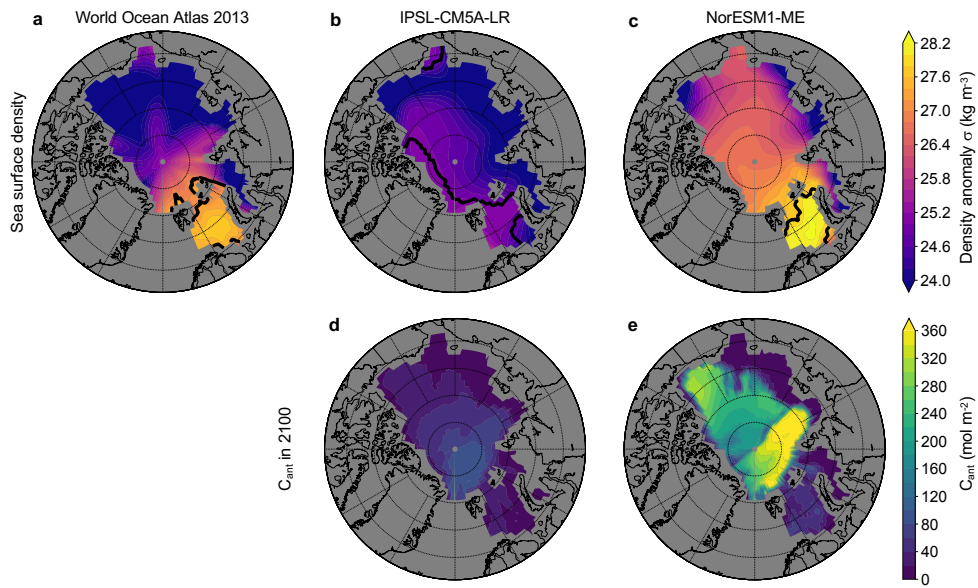
84 To reduce Arctic Ocean projection uncertainties associated with the anthropogenic carbon
 85 inventory and concurrent acidification, here we utilise the recent approach of emergent
 86 constraints^{11,21,22,23}. In order to constrain future ESM projection uncertainties, emergent
 87 constraints relate long-timescale climate sensitivities and impacts to observable properties,
 88 such as short-timescale climate variability or trends, across ESM ensembles. Emergent

89 constraints have previously been used to reduce the uncertainty, amongst other climate
90 projections, associated with Arctic summer sea ice¹¹, equilibrium climate sensitivity²² and
91 impacts on marine primary production²¹.

92

93 Here we show that across an ensemble of 11 ESMs (Table S1) there is a consistent relationship
94 between present-day Arctic Ocean maximum sea surface water density, the projected end-of-
95 century Arctic Ocean anthropogenic carbon inventory and the extent of ocean acidification
96 under RCP8.5 (Fig. 2, 3). All models performed simulations as part of the Coupled Model
97 Intercomparison Project Phase 5 (CMIP5). Present-day (1986-2005) maximum sea surface
98 density was calculated, for each model, as the mean of the 95th percentile of monthly surface
99 water densities in the Arctic. Across all models, these maximum density waters are primarily
100 located in the Barents Sea (Extended Data Figure 2). The anthropogenic carbon inventory was
101 calculated as the difference in integrated Arctic Ocean dissolved inorganic carbon between
102 RCP8.5 simulations and the respective pre-industrial control simulation of each model. While
103 projections of variables associated with ocean acidification ($\Omega_{\text{calc/arag}}$, pH and $p\text{CO}_2$) were
104 calculated from model outputs of total alkalinity, dissolved inorganic carbon, temperature,
105 salinity, total dissolved inorganic phosphorus and silicon and bias-corrected using GLODAPv2²⁴
106 (see Methods).

107



108

109 **Fig. 2. Arctic Ocean surface water density and the anthropogenic carbon inventory. a,**

110 Present-day annual-mean sea surface density from World Ocean Atlas 2013²⁵ and the **b,** IPSL-

111 CM5A-LR and **c,** NorESM1-ME models. Contours delineate regions that contribute to the

112 maximum surface density as defined by the 95th percentile densities. Vertically integrated

113 anthropogenic carbon (C_{ant}) projections in 2100 for the **d,** IPSL-CM5A-LR and **e,** NorESM1-ME

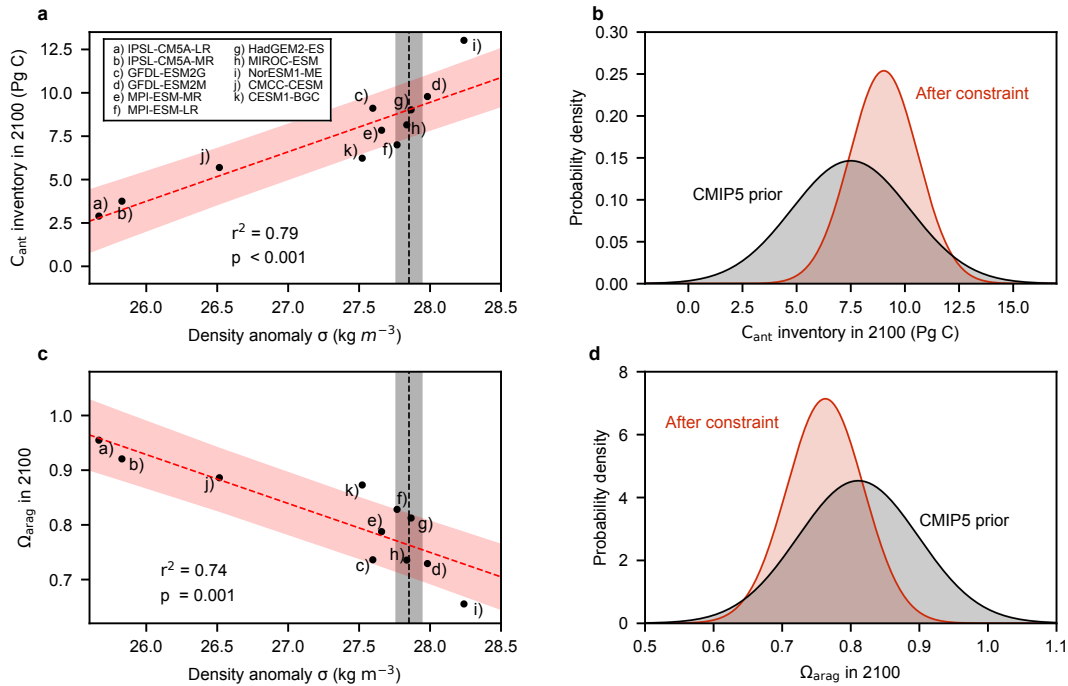
114 models. IPSL-CM5A-LR represents the ensemble minimum for both present-day maximum sea

115 surface density ($1025.67 \text{ kg m}^{-3}$) and projected C_{ant} inventory in 2100 (2.9 Pg C), while

116 NorESM1-ME is the ensemble maximum ($1028.24 \text{ kg m}^{-3}$ and 13.0 Pg C). The maximum sea

117 surface density from WOA 2013 is $1027.85 \text{ kg m}^{-3}$

118



119

120 **Fig. 3. Emergent constraints on the projected anthropogenic carbon inventory and future**
 121 **acidification. a**, The projected Arctic Ocean anthropogenic carbon inventory and **c**, basin-
 122 averaged Ω_{arag} in 2100 against present-day maximum sea surface density (95th percentile
 123 waters) for the ESM ensemble (black dots). Linear regression fits (red dashed lines) and the
 124 associated 68 % prediction intervals are shown, as are data-based estimates of present-day
 125 maximum sea surface density (black dashed lines) with the associated standard deviation (black
 126 shaded area). Probability density functions for the end-of-century **b**, Arctic Ocean
 127 anthropogenic carbon inventory and **d**, basin-averaged Ω_{arag} , before (black) and after (red) the
 128 emergent constraint is applied.

129

130

131 ESMs such as IPSL-CM5A-LR, which simulate lower than observed present-day Arctic Ocean
132 maximum surface densities, a proxy for Arctic deep-water formation (Extended Data Figure 3),
133 typically project lower end-of-century anthropogenic carbon inventories under RCP8.5 than
134 models such as NorESM1-ME, which simulate higher densities (Fig. 2). This emergent
135 relationship across the ESM ensemble is consistent at the scale of the Arctic Ocean basin, with
136 present-day maximum surface density exhibiting a strong relationship with end-of-century
137 depth integrated anthropogenic carbon inventories ($r^2=0.79$, $P < 0.001$; Fig. 3). Given the
138 dominance of anthropogenic carbon uptake in driving ocean acidification (Extended Data Figure
139 4), models with higher maximum sea surface density also exhibit stronger twenty-first century
140 reductions in basin-average Ω_{arag} ($r^2=0.74$, $P = 0.001$; Fig. 3), Ω_{calc} ($r^2=0.74$, $P = 0.001$; Extended
141 Data Figure 1) and pH ($r^2=0.77$, $P < 0.001$; Extended Data Figure 1). Observations of sea surface
142 density²⁵ were then used in combination with these multi-model relationships, to provide
143 emergent constraints on projections of Arctic Ocean anthropogenic carbon storage, and
144 concomitant acidification. Potential alternative constraints, such as present-day seasonal sea
145 ice extent, were found to be non-indicative of future Arctic Ocean anthropogenic carbon and
146 acidification across the ESM ensemble (Extended Data Figure 3).

147

148 Our emergent constraint increases projections of the end-of-century Arctic Ocean
149 anthropogenic carbon inventory from 7.5 ± 2.7 Pg C (CMIP5 multi-model mean) to 9.0 ± 1.6 Pg
150 C, with a 41 % reduction in uncertainty (Fig. 3). Similarly, average end-of-century Ω_{arag} and Ω_{calc}
151 are reduced from 0.81 ± 0.09 to 0.76 ± 0.06 and from 1.27 ± 0.14 to 1.19 ± 0.09 , respectively

152 (Fig. 3, Extended Data Figure 1). As such, the low bias of maximum sea surface density in 8 of 11
153 ESMs is indicative of an underestimation of projected anthropogenic carbon storage and
154 therefore future Arctic Ocean acidification in the CMIP5 multi-model mean.

155

156 The mechanisms underpinning the relationship between maximum surface densities and
157 anthropogenic carbon uptake are intrinsically related to Arctic Ocean circulation and dynamics.
158 The majority of intermediate and deep Arctic waters and the anthropogenic carbon they carry
159 are of Atlantic origin^{26,27}. The dominant net influx of anthropogenic carbon from the Atlantic
160 into the Arctic Ocean is through the Barents Sea Opening, as indicated by both data-based
161 estimates²⁸ ($41 \pm 8 \text{ Tg C yr}^{-1}$) and ocean carbon cycle models (21-48 Tg C yr⁻¹; Table S2). This
162 inflowing water is seasonally cooled in the Barents Sea via surface heat exchange and enriched
163 in salinity via brine rejection during the formation of sea ice^{29,30}. Consequently, during winter,
164 seawater density increases and water masses sink into the interior Arctic Ocean, mainly via the
165 St Anna Trough, where they supply most intermediate and deep waters^{26,27}. As such, the
166 present-day ability of ESMs to simulate the maximum surface densities that occur in the
167 Barents Sea, is highly indicative of their capacity to transport future anthropogenic carbon into
168 the Arctic interior.

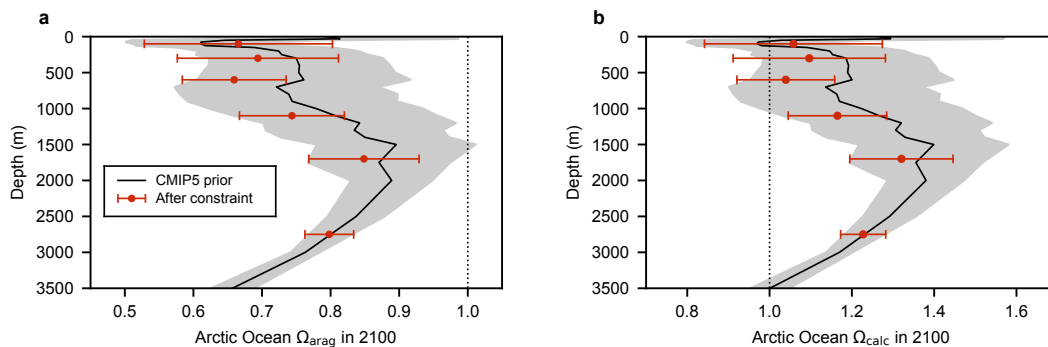
169

170 These mechanisms were further explored in historical (1870-2012) simulations of an ocean-only
171 carbon-cycle model (NEMO-PISCES), performed at three spatial resolutions¹⁹. These simulations
172 confirm the importance of Atlantic waters that flow into the Barents Sea, in determining net

173 changes in the Arctic Ocean anthropogenic carbon inventory (Table S2). They further show that
 174 across model spatial resolutions there is a strong positive relationship ($r^2=0.98$, $P = 0.08$; Fig. S1)
 175 between maximum surface density and the historical change in Arctic Ocean anthropogenic
 176 carbon inventory (Fig. S2). One of the principal drivers of the CMIP5 emergent relationship
 177 therefore appears to be variable ESM resolution and associated difficulties in resolving the
 178 transport of anthropogenic carbon into the Arctic basin at low resolutions¹⁹. Indeed, CMIP5
 179 ESMs with higher Arctic Ocean resolution typically project greater end-of-century
 180 anthropogenic carbon inventories ($r^2=0.44$, $P = 0.03$; Extended Data Figure 3).

181

182



183

184 **Fig. 4. Constrained end-of century Arctic Ocean vertical profiles of $\Omega_{\text{calc/arag}}$.** Multi-model mean
 185 vertical profiles of basin-averaged **a**, Ω_{arag} and **b**, Ω_{calc} in 2100 (black lines) with the associated
 186 standard deviation ($n=11$; grey shading). Constrained mean estimates of Ω_{arag} and Ω_{calc} (red
 187 dots) are shown for six different depth layers (0-200 m, 200-400 m, 400-800 m, 800-1400 m,
 188 1400-2000 m, 2000 m - bottom). The constrained estimates are shown at the mid-point of each
 189 layer, with error bars representing \pm one standard deviation.

190 Extending the emergent constraint approach from the entire Arctic basin to multiple vertical
191 depth integrals, we reduce uncertainties associated with projections of changing vertical
192 profiles of $\Omega_{\text{calc/arag}}$ (Fig. 4, Extended Data Figures 5, 6), pH and $p\text{CO}_2$ (Extended Data Figures 7,
193 8). Basin-wide emergent constraints on twenty-first century acidification are shown to be
194 predominantly driven by subsurface waters between 400 and 1400 m, with the strongest multi-
195 model relationship between present-day maximum surface density and end-of-century $\Omega_{\text{calc/arag}}$
196 found between 400 and 800 m ($r^2 = 0.84$, $P < 0.001$; Extended Data Figures 5, 6). In these
197 mesopelagic waters, end-of-century Ω_{arag} is reduced from a CMIP5 multi-model mean of $0.75 \pm$
198 0.15 to 0.66 ± 0.08 , with end-of-century Ω_{calc} reduced from 1.18 ± 0.23 to 1.04 ± 0.12 . A
199 consequence of our constrained vertical profiles of marine chemistry is that the lowest average
200 end-of-century $\Omega_{\text{calc/arag}}$ will likely not occur in Arctic Ocean surface waters, as previously
201 expected^{3,8}, but between 400-800 m (Fig. 4). In these mesopelagic waters, the probability of
202 end-of-century $\Omega_{\text{calc}} < 1$ and $\Omega_{\text{arag}} < 0.75$ is increased from 23% and 51% respectively in the
203 CMIP5 prior to 37% and 88% respectively after the constraint is applied (Extended Data Table
204 1).

205

206 In the upper Arctic Ocean (0-200 m), present-day maximum surface density exhibits limited
207 relationship with end-of-century $\Omega_{\text{calc/arag}}$ across the models (Extended Data Figures 5, 6) and
208 emergent constraints offer no reduction in projection uncertainties (Fig. 4). This is to be
209 expected in waters where deep-water formation has little impact on marine chemistry.
210 Similarly, below 2000 m where there is limited change in the anthropogenic carbon inventory

211 and associated marine chemistry this century (Fig. 1, Extended Data Figure 1), there is no
212 relationship between present-day maximum surface density and end-of-century $\Omega_{\text{calc/arag}}$
213 (Extended Data Figures 5, 6).

214

215 The constrained estimates of greater twenty-first century Arctic Ocean acidification presented
216 here, have major implications for sensitive Arctic marine ecosystems already exposed to
217 multiple climatic stressors. Enhanced subsurface acidification is likely to have negative
218 consequences on organisms that both permanently inhabit the mesopelagic and those that
219 utilise it as part of seasonal or diel vertical migrations³¹. The suitable habitat available to
220 keystone species such as the aragonitic pteropod *Limacina helicina* is likely to decline to a
221 greater extent than previously anticipated given its sensitivity to Ω_{arag} ³², with negative
222 consequences for dependent pelagic food webs^{33,34,35}. Meanwhile, undersaturation with
223 respect to calcite is likely to have major consequences for calcite forming Arctic
224 coccolithophores³⁶ and foraminifera³⁷. Finally, our estimates of higher end-of century Arctic
225 Ocean $p\text{CO}_2$, which increases from $1070 \pm 239 \mu\text{atm}$ at depths of 400-800 m to 1216 ± 121
226 μatm under the constraint (Extended Data Figure 8), is likely to negatively affect the growth,
227 survival³⁸ and behaviour^{39,40} of ecologically important fish such as polar cod.

228

229 **References**

- 230 1. Haugan, P. M. & Drange, H. Effects of CO₂ on the ocean environment. *Energy Convers.*
231 *Mgmt* **37**, 1019–1022 (1996).
- 232 2. Orr, J. C. et al. Anthropogenic ocean acidification over the twenty-first century and its
233 impact on calcifying organisms. *Nature* **437**, 681–686 (2005).
- 234 3. Steinacher, M., Joos, F., Frolicher, T. L., Plattner, G. K. & Doney, S. C. Imminent ocean
235 acidification in the Arctic projected with the NCAR global coupled carbon cycle-climate model.
236 *Biogeosciences* **6**, 515–533 (2009).
- 237 4. Fabry, V. J., McClintock, J. B., Mathis, J. T. & Grebmeier, J. M. Ocean acidification at high
238 latitudes: The bellweather. *Oceanography* **22**, 160–171 (2009).
- 239 5. Gattuso, J.-P. & Hansson, L. *Ocean Acidification* (Oxford Univ. Press, 2011).
- 240 6. Riebesell U, Gattuso JP, Thingstad TF, Middelburg JJ. Preface “Arctic ocean acidification:
241 pelagic ecosystem and biogeochemical responses during a mesocosm study”. *Biogeosciences*
242 **10**(8), 5619–5626 (2013).
- 243 7. AMAP, 2018. AMAP Assessment 2018: Arctic Ocean Acidification. Arctic Monitoring and
244 Assessment Programme (AMAP), Tromsø, Norway. vi+187pp
- 245 8. Steiner, N. S., Christian, J. R., Six, K. D., Yamamoto, A., & Yamamoto-Kawai, M. Future
246 ocean acidification in the Canada Basin and surrounding Arctic Ocean from CMIP5 earth system
247 models. *Journal of Geophysical Research: Oceans* **119**(1), 332–347 (2014).

- 248 9. Kwiatkowski, L. & Orr, J.C. Diverging seasonal extremes for ocean acidification during
249 the twenty-first century. *Nature Climate Change* **8**(2), 141 (2018)
- 250 10. Collins, M. et al. in *Climate Change 2013: The Physical Science Basis* (eds Stocker, T. F. et
251 al.) 1029–1136 (IPCC, Cambridge Univ. Press, 2013).
- 252 11. Boé, J., Hall, A. & Qu, X. September sea ice cover in the Arctic Ocean projected to vanish
253 by 2100. *Nature Geosci.* **2**, 341–343 (2009).
- 254 12. Kroeker, K. J., Kordas, R. L., Crim, R. N. & Singh, G. G. Meta-analysis reveals negative yet
255 variable effects of ocean acidification on marine organisms. *Ecol. Lett.* **13**, 1419–1434 (2010).
- 256 13. Langdon, C. & Atkinson, M. Effect of elevated $p\text{CO}_2$ on photosynthesis and calcification
257 of corals and interactions with seasonal change in temperature/irradiance and nutrient
258 enrichment. *J. Geophys. Res.* **110**, C09S07 (2005).
- 259 14. Bednaršek, N., Tarling, G. A., Bakker, D. C., Fielding, S. & Feely, R. A. Dissolution
260 dominating calcification process in polar pteropods close to the point of aragonite
261 undersaturation. *PLoS ONE* **9**(10), e109183 (2014).
- 262 15. Albright, R. et al. Reversal of ocean acidification enhances net coral reef calcification.
263 *Nature* **531**, 362–365 (2016).
- 264 16. Yamamoto-Kawai, M., McLaughlin, F. A., Carmack, E. C., Nishino, S. & Shimada, K.
265 Aragonite undersaturation in the Arctic Ocean: Effects of ocean acidification and sea ice melt.
266 *Science* **326**, 1098–1100 (2009).

- 267 17. Riahi, K. et al. RCP 8.5—A scenario of comparatively high greenhouse gas emissions.
268 *Clim. Change* **109**, 33–57 (2011).
- 269 18. Feely, R. A., Doney, S. C. & Cooley, S. R. Ocean acidification: Present conditions and
270 future changes in a high-CO₂ world. *Oceanography* **22**, 36–47 (2009).
- 271 19. Terhaar, J., Orr, J. C., Gehlen, M., Ethé, C., and Bopp, L. Model constraints on the
272 anthropogenic carbon budget of the Arctic Ocean. *Biogeosciences* **16**, 2343–2367 (2019).
- 273 20. Frolicher, T. L., Rodgers, K., Stock, C. & Cheung, W. W. L. Sources of uncertainties in 21st
274 century projections of potential ocean ecosystem stressors. *Global Biogeochem. Cycles* **30**,
275 1224–1243 (2016).
- 276 21. Kwiatkowski, L. et al. Emergent constraints on projections of declining primary
277 production in the tropical oceans. *Nat. Clim. Chang.* **7**, 355–358 (2017).
- 278 22. Cox, P. et al. Sensitivity of tropical carbon to climate change constrained by carbon
279 dioxide variability. *Nature* **494**, 341–344 (2013)
- 280 23. Eyring, V. et al. Taking climate model evaluation to the next level. *Nat. Clim. Chang.* **9**,
281 102–110 (2019).
- 282 24. Lauvset, S. K. et al. A new global interior ocean mapped climatology: the 1°×1° GLODAP
283 version 2. *Earth Syst. Sci. Data* **8**, 325–340 (2016).
- 284 25. Boyer, T. P. et al. *World Ocean Database 2013* (Silver Spring, accessed March 2019).
- 285 26. Rudels, B., Jones, E. P., Anderson, L. G., & Kattner, G. On the intermediate depth waters

286 of the Arctic Ocean. *The polar oceans and their role in shaping the global environment*, **85**, 33-
287 46 (1994).

288 27. Rudels, B., Muench, R. D., Gunn, J., Schauer, U., & Friedrich, H. J. Evolution of the Arctic
289 Ocean boundary current north of the Siberian shelves. *J. Marine Syst.*, **25**(1) . (2001). 77-99.

290 28. Jeansson, E. et al. The Nordic Seas carbon budget: Sources, sinks, and uncertainties.
291 *Global Biogeochem. Cy.*, **25**(4). (2011)

292 29. Midttun, Lars. "Formation of dense bottom water in the Barents Sea." *Deep Sea Res.*
293 **32**.10, 1233-1241 (1985)

294 30. Smedsrud, L. H. et al. The role of the Barents Sea in the Arctic climate system. *Rev.*
295 *Geophys.* **51**, 415–449 (2013).

296 31. Berge, J. et al. In the dark: A review of ecosystem processes during polar night. *Prog.*
297 *Oceanogr.* **139**, 258–271 (2015).

298 32. Comeau, S., Jeffree, R., Teyssie, J. L. & Gattuso, J. P. Response of the Arctic pteropod
299 *Limacina helicina* to projected future environmental conditions. *PLoS ONE* **5**, e11362 (2010).

300 33. Hunt, B. P. V. et al. Pteropods in Southern Ocean ecosystems. *Prog. Oceanogr.* **78**, 193–
301 221 (2008).

302 34. Armstrong, J. L. et al. Distribution, size, and interannual, seasonal and diel food habits of
303 northern Gulf of Alaska juvenile pink salmon, *Oncorhynchus gorbuscha*. *Deep-Sea Res. Pt. II* **52**,
304 247–265 (2005).

- 305 35. Karnovsky, N. J., Hobson, K. A., Iverson, S., & Hunt Jr, G. L. Seasonal changes in diets of
306 seabirds in the North Water Polynya: a multiple-indicator approach. *Mar. Ecol. Prog. Ser.*, **357**,
307 291–299 (2008).
- 308 36. Kottmeier, D. M., Rokitta, S. D., & Rost, B. H⁺-driven increase in CO₂ uptake and decrease
309 in HCO₃⁻ uptake explain coccolithophores' acclimation responses to ocean acidification. *Limnol.*
310 *Oceanogr.* **61**, 2045–2057 (2016)
- 311 37. Davis, C. V. et al. Ocean acidification compromises a planktic calcifier with implications
312 for global carbon cycling. *Sci. Rep.* **7**, 2225 (2017)
- 313 38. Frommel, A. Y. et al. Severe tissue damage in Atlantic cod larvae under increasing ocean
314 acidification. *Nature Clim. Change* **2**, 42–46 (2012).
- 315 39. Schmidt, M. et al. Differences in neurochemical profiles of two gadid species under
316 ocean warming and acidification. *Front. Zool.* **14**, 49 (2017).
- 317 40. Kunz, K. et al. Aerobic capacities and swimming performance of polar cod (*Boreogadus*
318 *saida*; lepechin) under ocean acidification and warming conditions. *J. Exp. Biol.* **221** (2018)

319

320 **Methods**

321

322 **Earth System Models**

323 In the ensemble of 11 Coupled Model Intercomparison Project Phase 5 (CMIP5) ESMs (Table S1)
324 utilised, all included coupled ocean biogeochemistry schemes and have been extensively
325 applied within the context of both climate and ocean biogeochemical projections^{8,9,21}. A single
326 ensemble member was utilised for each ESM. Prognostic annual model output fields of
327 dissolved inorganic carbon, total alkalinity, dissolved inorganic phosphorus and silicon,
328 temperature, and salinity were taken across all vertical depth levels in the Arctic Ocean, limited
329 by the Fram Strait, the Barents Sea Opening, the Bering Strait and the Canadian Arctic
330 Archipelago^{19,41}. Monthly sea surface density outputs were taken over the same domain. All
331 output fields were regridded on a regular 1°×1° grid to facilitate multi-model analysis.

332 The anthropogenic carbon inventory was calculated as the difference between dissolved
333 inorganic carbon in historical (1850-2005) simulations merged with RCP8.5 (2006-2100) and the
334 concurrent pre-industrial control (piControl) simulations. As such, any model drift in deep-
335 ocean dissolved inorganic carbon was directly accounted for. Across all models, the simulated
336 present-day (2005) Arctic Ocean anthropogenic carbon inventory (0.2-2.4 Pg C) is below the
337 data-based estimate of 2.5-3.3 Pg C⁴².

338 All carbonate chemistry variables were calculated offline from dissolved inorganic carbon, total
339 alkalinity, temperature, salinity and where available, dissolved inorganic phosphorus and
340 silicon, over 1850-2100 using mocsy2.0⁴³ and the equilibrium constants recommended for best

341 practices⁴⁴. To account for carbonate chemistry biases in the present-day mean state of the
342 ESMs⁸, model anomalies of all input variables relative to 2002 were combined with the data-
343 based GLODAPv2 observational product²⁴ which is normalised to the year 2002. Model
344 anomalies were corrected for potential model drift using concurrent piControl simulations. All
345 grid cells with GLODAPv2 observational coverage (~65 % of Arctic Ocean volume) were utilised.
346 Basin-wide averages of Ω_{arag} , Ω_{calc} , pH and $p\text{CO}_2$ were weighted based on grid cell volumes.

347 The Arctic Ocean present-day maximum sea surface density was calculated for each ESM from
348 1986-2005 monthly sea surface density climatologies, constructed from temperature and
349 salinity outputs. Maximum present-day sea surface density was defined as the mean density of
350 the densest 5 % of Arctic surface waters (95th percentile waters) throughout the climatological
351 year. Maximum present-day sea surface density consistently occurs in the Barents Sea, across
352 both observations and the ESM ensemble. Given the importance of the Barents Sea in supplying
353 intermediate and deep Arctic waters^{26,27,29,30}, maximum sea surface density, as defined, is
354 indicative of the bowl of ventilated Arctic waters. Across all models, the volume of Arctic Ocean
355 waters that are lighter than the maximum sea surface density increases with the maximum sea
356 surface density ($r^2 = 0.59$, $P=0.006$; Extended Data Figure 3).

357 In addition to sea surface density, alternative potential constraints on the projected Arctic
358 Ocean anthropogenic carbon inventory and associated acidification were assessed. The
359 representation of Arctic sea ice extent⁴⁵ and intermediate North Atlantic water masses⁴⁶ varies
360 substantially across the CMIP5 ensemble. However, both present-day sea-ice extent (Extended
361 Data Figure 3) and the properties of North Atlantic water masses were found to be non-

362 indicative of projected Arctic Ocean carbon uptake and associated acidification across the
363 model ensemble.

364 An assessment of the potential for model internal variability to influence the Arctic Ocean
365 emergent constraint approach is provided in the supplementary material. Utilising four
366 ensemble members of the IPSL-CM5A-LR model, the internal variability of present-day sea
367 surface density and projected anthropogenic carbon inventory is shown to be highly limited
368 compared to the differences across the CMIP5 models (Extended Data Figure 9).

369

370 **Ocean-only simulations**

371 Hindcast ocean-biogeochemical simulations of the NEMO-PISCES model⁴⁷ that have been
372 previously published¹⁹ are used in this study to explore the mechanisms behind the identified
373 Arctic Ocean emergent constraint. The model is run at a nominal resolution of 0.5° from 1870
374 to 1958 and at three different nominal horizontal resolutions from 1958 to 2012: 2° (ORCA2),
375 0.5° (ORCA05), and 0.25° (ORCA025). All three model configurations are forced with the
376 DRAKKAR historical reanalysis forcing dataset⁴⁸ and therefore only differ in horizontal
377 resolution and the associated diffusion scheme and coefficients.

378

379

380

381 **Observational constraints**

382 Observational sea surface density constraints were derived from the World Ocean Atlas 2013
383 temperature and salinity climatologies²⁵. The maximum Arctic Ocean sea surface density was
384 then calculated in the same manner as for the ESM ensemble.

385 The uncertainty associated with Arctic Ocean maximum sea surface density observational
386 constraints was estimated using standard propagation of uncertainty and combining (1) the
387 published standard deviations of sea surface temperature and salinity for each grid cell and
388 each month in WOA2013 to derive standard deviations for sea surface density, and (2) the
389 standard deviation obtained when computing the weighted mean of 95th percentile density
390 waters.

391 Arctic Ocean salinity in World Ocean Atlas 2013 was recently evaluated against available in-situ
392 data⁴⁹. This comparison suggests that salinity observations in the World Ocean Atlas may have a
393 small negative bias in the Barents Sea that may contribute to a negative density bias.
394 Corroboration and correction of such a bias would, if anything, result in a minor increase in our
395 constrained estimates of projected Arctic Ocean anthropogenic carbon and associated
396 acidification.

397

398 **Probability density functions of anthropogenic carbon and ocean acidification**

399 Probability density functions (PDFs) of anthropogenic carbon storage and basin-averaged Ω_{arag} ,
400 Ω_{calc} and pH in 2100 were calculated for the unconstrained (prior) CMIP5 ensemble and the

401 emergent constraints. The prior PDF was derived assuming all models were equally likely and
402 sampled from a Gaussian distribution. The constrained PDFs were calculated as the normalised
403 product of the conditional PDF of the emergent relationship and the PDF of the observational
404 constraint following previously established methodologies^{21,22,50}.

405

406

407 **References (Methods)**

- 408 41. Bates, N. R. & Mathis, J. T. The Arctic Ocean marine carbon cycle: Evaluation of air-sea
409 CO₂ exchanges, ocean acidification impacts and potential feedbacks. *Biogeosciences* **6**, 2433–
410 2459 (2009).
- 411 42. Tanhua, T. et al. Ventilation of the Arctic Ocean: mean ages and inventories of
412 anthropogenic CO₂ and CFC-11. *J. Geophys. Res.* **114** (2009).
- 413 43. Orr, J. C. & Epitalon, J.-M. Improved routines to model the ocean carbonate system:
414 mocsy 2.0. *Geosci. Model Dev.* **8**, 485–499 (2015).
- 415 44. Dickson, A. G., Sabine, C. L. & Christian, J. R. (eds) *Guide to Best Practices For Ocean CO₂*
416 *Measurements* 191 (PICES Special Publication 3, 2007).
- 417 45. Shu, Q., Song, Z. & Qiao, F. Assessment of sea ice simulations in the CMIP5 models.
418 *Cryosphere* **9**, 399–409 (2015).
- 419 46. Shu, Q., Wang, Q., Su, J., Li, X., & Qiao, F. Assessment of the Atlantic water layer in the
420 Arctic Ocean in CMIP5 climate models. *Clim. Dyn.* **53** 5279-5291 (2019).
- 421 47. Aumont, O. & Bopp, L. Globalizing results from ocean in situ iron fertilization studies.
422 *Glob. Biogeochem. Cycles* **20**, GB2017 (2006).
- 423 48. Brodeau, L., Barnier, B., Treguier, A. M., Penduff, T. & Gulev, S. An ERA40-based
424 atmospheric forcing for global ocean circulation models. *Ocean Model.* **31**, 88–104 (2010).
- 425 49. Xie, J., Raj, R. P., Bertino, L., Samuelsen, A., & Wakamatsu, T. Evaluation of Arctic Ocean
426 surface salinities from SMOS and two CMEMS reanalyses against in situ data sets. *Ocean Sci.* **15**,

427 1191–1206 (2019).

428 50. Wenzel, S., Cox, P. M., Eyring, V. & Friedlingstein, P. Emergent constraints on climate-
429 carbon cycle feedbacks in the CMIP5 Earth system models. *J. Geophys. Res. Biogeosciences* **119**,
430 2013JG002591 (2014).

431

432

433

434 **Acknowledgements**

435 This study was funded by the H2020 C-CASCADES grant (ref 643052), the H2020 CRESCENDO
436 grant (ref 641816), the H2020 4C grant (ref 821003), the Agence Nationale de la Recherche
437 grant ANR-18-ERC2-0001-01 (CONVINCE), the MTES/FRB Acidoscope project and the ENS-
438 Chanel research chair. We acknowledge the World Climate Research Programme's Working
439 Group on Coupled Modelling, which is responsible for CMIP. For CMIP the US Department of
440 Energy's Program for Climate Model Diagnosis and Intercomparison provided coordinating
441 support and led the development of software infrastructure in partnership with the Global
442 Organisation for Earth System Science Portals. The authors also thank the IPSL modelling group
443 for the software infrastructure, which facilitated CMIP5 analysis, Jean-Marc Molines, Laurent
444 Brodeau, and Bernard Barnier for developing the DRAKKAR ORCA05 and ORCA025 global
445 configurations of NEMO and Jennifer Simeon, Christian Ethé, Marion Gehlen, and James C. Orr
446 for the implementation of NEMO-PISCES within these configurations.

447

448 **Author contributions**

449 This study was conceived by all coauthors. J.T. performed the model output analysis and
450 produced the figures, with help from L.K. and L.B. All authors contributed ideas, discussed the
451 results and wrote the manuscript.

452

453

454 **Author information**

455 The authors declare no competing financial interests. Correspondence and requests for
456 materials should be addressed to J.T (jens.terhaar@climate.unibe.ch).

457

458 **Data availability**

459 The Earth system model output used in this study is available via the Earth System Grid
460 Federation (<https://esgf-node.ipsl.upmc.fr/projects/esgf-ipsl/>). Observations from the World
461 Ocean Atlas 2013 (<https://www.nodc.noaa.gov/OC5/woa18/>) and GLODAPv2
462 (https://www.nodc.noaa.gov/ocads/oceans/GLODAPv2_2019/) are available via the National
463 Oceanic and Atmospheric Administration. Prior to publication, the output of ocean-only NEMO-
464 PISCES simulations is openly accessible on the ODATIS-supported center 'Sea scientific open
465 data publication' (<https://doi.org/10.17882/72239>).

466

467 **Code availability**

468 The Python module 'statsmodels' (<https://www.statsmodels.org/stable/index.html>) was used for linear
469 regression and the calculation of prediction intervals. The mocsy2.0 routines were used to calculate the
470 ocean carbonate system variables (<http://ocmip5.ipsl.jussieu.fr/mocsy/>). The Climate Data Operators
471 (CDO) were used for regridding of CMIP5 model output (<https://code.mpimet.mpg.de/projects/cdo/>).
472 The code for the NEMO ocean model version 3.2 is available under CeCILL license online
473 (<http://www.nemo-ocean.eu>).